Dynamical properties of a strongly correlated model for quarter-filled layered organic molecular crystals

Jaime Merino

Max-Planck-Institut für Festkörperforschung, D-70506, Stuttgart, Germany

Andrés Greco

Facultad de Ciencias Exactas Ingeniería y Agrimensura e Instituto de Física Rosario (UNR-CONICET), Rosario, Argentina

Ross H. McKenzie

Department of Physics, University of Queensland, Brisbane 4072, Australia

Matteo Calandra

Laboratoire de Minéralogie-Cristallographie, case 115, 4 Place Jussieu, 75252 Paris Cedex 05, France

The dynamical properties of an extended Hubbard model, which is relevant to quarter-filled layered organic molecular crystals, are analyzed. We have computed the dynamical charge correlation function, spectral density, and optical conductivity using Lanczos diagonalization and large-N techniques. As the ratio of the nearest-neighbor Coulomb repulsion, V, to the hopping integral, t, increases there is a transition from a metallic phase to a charge-ordered phase. Dynamical properties close to the ordering transition are found to differ from the ones expected in a conventional metal. Large-N calculations display an enhancement of spectral weight at low frequencies as the system is driven closer to the charge-ordering transition in agreement with Lanczos calculations. As V is increased the charge correlation function displays a collective mode which, for wave vectors close to (π,π), increases in amplitude and softens as the charge-ordering transition is approached. We propose that inelastic x-ray scattering be used to detect this mode. Large-N calculations predict superconductivity with d_{xy} symmetry close to the ordering transition. We find that this is consistent with Lanczos diagonalization calculations, on lattices of 20 sites, which find that the binding energy of two holes becomes negative close to the charge-ordering transition.

I. INTRODUCTION

The competition between charge-ordered, metallic, and superconducting phases is relevant to a broad range of strongly correlated electron materials. For example, in the vanadium bronze β-$Na_{0.33}V_2O_5$, superconductivity appears close to a charge-ordered phase under an applied external pressure.[1] The appearance of a pseudogap in oxygenated samples of $Nd_{1.85}Ce_{0.15}CuO_{4+y}$ has been suggested to be due to charge ordering.[2] Quarter-filled layered organic materials such as the bis-ethylenedithio-tetrathiafulvalene (BEDT-TTF) family of organic molecular crystals[3] with the θ and β'' molecular stacking patterns also display a subtle competition of metallic, insulating, charge-ordered, and superconducting phases.[4] Supercon-ductivity in organic compounds is usually found in close proximity to ordered insulating phases.[3] For example, κ-$(BEDT$-$TTF)_2Cu[N(CN)_2]Cl$ is an antiferromag-netic Mott insulator which becomes supercon-ducting under pressure.[5] Superconducting θ-$(ET)_2I_3$ and β''-$(BEDT$-$TTF)_3Cl_2(H_2O)_2$ are close to charge-ordered phases.[6] Superconductivity occurs in the quasi-one-dimensional Bechgaard salts, (tetramethyl tetraselena ful-valene) $TMTSF_2X$, when a spin-density wave is suppressed. It is then important to understand the connection of the su-perconducting state to the nearby ordered phases and analyze the effect of the fluctuations associated with the ordering transition on the normal metallic phase.

Several anomalous properties have been observed close to the charge-ordering transition in quarter-filled organic con-ductors. (i) Suppression of Drude weight and enhancement of optical spectra at low frequencies at about 500–1000 cm^{-1} in metallic θ (Refs. 8,7) β'' (Ref. 9) and α salts[10] at low temperatures. (ii) The temperature dependence of the resistivity may be different from Fermi-liquid behav-ior, in particular, the resistivity can increase as the tempera-ture is decreased just before becoming superconducting (see the Table in Ref. 6). Previously we have explored, using slave bosons, the possibility of superconductivity[6] and the metal-insulator transition[11] in the quarter-filled extended Hubbard model. Here, we concentrate on the dynamical properties in the metallic phase close to the charge-ordering transition. We find that due to the scattering of electrons from charge fluctuations with (π,π) wave vector, dynamical and transport properties display behavior different from that ex-pected in a typical metal. For instance, a strong suppression of quasiparticle weight as well as enhancement of spectral weight at low but finite frequencies takes place as the charge-ordering transition is approached from the metallic side. Also we examine the possibility of superconductivity mediated by short-range charge fluctuations close to the transition. We find that superconductivity with d_{xy} symmetry is possible close to the charge-ordering transition. We note that the present analysis is similar in spirit to those that aim to un-derstand the effect of spin fluctuations on the metallic phase

68 245121-1

and the possibility of superconductivity mediated by them[12] in high-T_c compounds, κ-(BEDT-TTF)$_2$X (Ref. 13), heavy fermions,[14] and ruthenates.[15]

In this paper we study the quarter-filled extended Hubbard model combining two techniques: large-N and Lanczos diagonalization on small clusters which complement each other. The comparison of a semianalytical approach with exact results leads to a deeper understanding of the numerical findings. It also shows which results obtained within the large-N approach are solid and which are weak. This paper is organized as follows. In Sec. II, we introduce an extended Hubbard model to describe the electronic properties of quarter-filled layered molecular crystals. We also review the path-integral formalism written in terms of Hubbard operators and the large-N expansion introduced to compute electronic properties of the model. In Sec. III, we show results for the dynamical charge correlation function, spectral density, and optical conductivity computed with Lanczos diagonalization comparing them with large-N results. In Sec. IV we discuss our results contrasting them with available experimental data on the quarter-filled organics. Section V is devoted to the possibility of having superconductivity in the model.

II. DYNAMICAL PROPERTIES IN THE U-INFINITE LIMIT: LARGE-N APPROACH

We consider an extended Hubbard model at one-quarter filling on a square lattice. This has been argued to be the simplest model needed to understand the electronic properties of the layered molecular crystals with the θ and β'' molecular arrangements within each layer.[4] The Hamiltonian is

$$H = -t \sum_{\langle ij \rangle, \sigma} (c_{i\sigma}^\dagger c_{j\sigma} + c_{j\sigma}^\dagger c_{i\sigma}) + U \sum_i n_{i\uparrow} n_{i\downarrow}$$

$$+ V \sum_{\langle ij \rangle} n_i n_j - \mu \sum_{i\sigma} n_{i\sigma}, \qquad (1)$$

where U and V are the on-site and the nearest-neighbors Coulomb repulsion, respectively, and $c_{i\sigma}^\dagger$ creates an electron of spin σ at site i. In the limit $U \gg V \gg t$ the ground state is insulating with a checkerboard charge-ordered pattern.[4] For $U \to \infty$ and $V = 0$, the system is expected to be metallic as it is quarter filled. Evaluation of the Drude weight by Lanczos techniques suggests that a metal-insulator transition takes place at a finite value of $V_c \approx 2.2t$ for a sufficiently large value[11] of $U = 10t$.

We now introduce the Hubbard operators

$$X_i^{0\sigma} = (1 - c_{i\bar\sigma}^\dagger c_{i\bar\sigma}) c_{i\sigma}, \quad X_i^{\sigma 0} = (X_i^{0\sigma})^\dagger, \quad X_i^{\sigma\sigma'} = c_{i\sigma}^\dagger c_{i\sigma'}. \qquad (2)$$

The five Hubbard $\hat{X}_i$ operators $X_i^{\sigma\sigma'}$ and X_i^{00} are boson-like and the four Hubbard $\hat{X}$ operators $X_i^{\sigma 0}$ and $X_i^{0\sigma}$ are fermionlike. The names fermionlike and bosonlike come from the fact that Hubbard operators do not verify the usual fermionic and bosonic commutation relations.[16]

In the U-infinite limit, the Hamiltonian (1) ($t-J-V$ model with $J=0$) can be written in terms of Hubbard operators as

$$H(X) = \sum_{\langle ij \rangle, \sigma} t_{ij} X_i^{\sigma 0} X_j^{0\sigma} + \sum_{\langle ij \rangle, \sigma} V_{ij} X_i^{\sigma\sigma} X_j^{\bar\sigma\bar\sigma} - \mu \sum_{i,\sigma} X_i^{\sigma\sigma}, \qquad (3)$$

where μ is the chemical potential. The Hubbard operators in this limit satisfy the completeness condition

$$X_i^{00} + \sum_\sigma X_i^{\sigma\sigma} = 1, \qquad (4)$$

which is equivalent to imposing that "double occupancy" at each site is forbidden.

There are two main difficulties in the calculation of physical quantities using Hamiltonian (1): the complicated commutation rules of the Hubbard operators[16] and the fact that there is no small parameter in the model. A popular method for handling the former difficulty is to use slave particles. For instance, within the slave boson method,[17] the original fermionic $X^{0\sigma}$ operator is decoupled as $X^{0\sigma} = b^\dagger f_\sigma$, where b and f are usual boson and fermion operators, respectively. The second difficulty can be dealt with by using a nonperturbative technique (which we will use in the present paper) based on a large-N expansion, where N is the number of electronic degrees of freedom per site and $1/N$ is assumed to be a small parameter. At one-quarter filling (which is the main interest in this paper), we expect the large-N approach to be a good approximation. This has been shown in the overdoped regime of high-T_c cuprates.[18]

Hamiltonian (1) has been treated via large N in a slave boson representation in Ref. 17 for $V = 0$, and in the context of quarter-filled layered organic superconductors ($V \neq 0$) in Ref. 4. Here, we concentrate on the dynamical properties of Hamiltonian (1), using the recently developed large-N expansion.[19] This method is based on a path-integral representation of the Hubbard X operators which is written in terms of Grassmann and usual bosonic variables associated with fermilike and bosonlike operators, respectively. In doing this, additional constraints are needed to make these field variables behave as Hubbard operators (satisfying their associated algebra), as they should. Although this may seem a great complication in the theory, in fact it avoids introducing any decoupling scheme of the original Hubbard operators, as in slave boson representations. For completeness we will summarize the framework used in the diagrammatic expansion developed in Ref. 19.

Our starting point is the partition function Z written in the Euclidean form:

$$Z = \int \mathcal{D}X_i^{\alpha\beta} \delta\left[X_i^{00} + \sum_\sigma X_i^{\sigma\sigma} - 1 \right] \delta\left[X_i^{\sigma\sigma'} - \frac{X_i^{\sigma 0} X_i^{0\sigma'}}{X_i^{00}} \right]$$

$$\times (\text{sdet} M_{AB})_i^{1/2} \exp\left(- \int d\tau L_E(X, \dot{X}) \right). \qquad (5)$$

The Euclidean Lagrangian $L_E(X, \dot{X})$ in Eq. (5) is

$$L_E(X,\dot{X}) = \frac{1}{2} \sum_{i,\sigma} \frac{(\dot{X}_i^{0\sigma} X_i^{\sigma 0} + \dot{X}_i^{\sigma 0} X_i^{0\sigma})}{X_i^{00}} + H(X). \quad (6)$$

It is worth noting at this point that the path-integral representation of the partition function (5) looks different to that usually found in other solid-state problems. The measure of the integral contains additional constraints as well as a superdeterminant $(\text{sdet} M_{AB})_i^{1/2}$. Also the kinetic term of the Lagrangian (6) is nonpolynomial. The determinant reads

$$(\text{sdet} M_{AB})_i^{1/2} = 1/\frac{1}{(-X^{00})^2}, \quad (7)$$

and is formed by all the constraints of the theory. Note that $(\text{sdet} M_{AB})_i^{1/2}$ is not proportional to $(-X^{00})^2$, because the theory is constrained in a supersymmetric sense where boson and fermion determinants must be treated in different ways (see Ref. 19 for more details about the path-integral formalism for Hubbard operators). The constraints appearing in the theory are necessary in order to recover the correct algebra of the original Hubbard operators. In Eq. (10) we show how to treat this determinant through the use of a large-N expansion.

We now discuss the main steps needed to introduce a large-N expansion of the partition function (5). First, we integrate over the boson variables $X^{\sigma\sigma'}$ using the second δ function in Eq. (5). We extend the spin index $\sigma = \pm$ to a new index p running from 1 to N. In order to get a finite theory in the $N \to \infty$ limit, we rescale the hopping t_{ij} to t_{ij}/N and V_{ij} to V_{ij}/N. In doing so, note that t_{ij}/N (rather than t_{ij}) should be fitted to band-structure calculations. The completeness

condition is enforced by exponentiating: $X_i^{00} + \Sigma_p X_i^{pp} = N/2$, the N-extended completeness condition, with the help of Lagrangian multipliers λ_i. From this completeness condition we can see that the charge operator X^{00} is O(1) in the $1/N$-expansion, while the operator X^{pp} is O(1/N). As a consequence of this, the large N approach presented here weakens the effective spin interaction compared to the one associated with the charge degrees of freedom. For instance, through O(1/N) we find collective excitations in the charge correlation function but not in the spin susceptibility.

We write the boson fields in terms of static mean-field values (r_0, λ_0) and dynamic fluctuations

$$X_i^{00} = N r_0 (1 + \delta R_i),$$

$$\lambda_i = \lambda_0 + \delta\lambda_i, \quad (8)$$

and, finally, we make the following change of variables:

$$f_{ip}^+ = \frac{1}{\sqrt{N r_o}} X_i^{p0},$$

$$f_{ip} = \frac{1}{\sqrt{N r_o}} X_i^{0p}, \quad (9)$$

where f_{ip}^+ and f_{ip} are Grassmann variables.

Introducing the above change of variables [Eqs. (8) and (9)] into Eq. (6), and after expanding the denominator appearing in Eq. (6), we arrive at the following effective Lagrangian:

$$L_{eff} = -\frac{1}{2} \sum_{i,p} (\dot{f}_{ip} f_{ip}^+ + \dot{f}_{ip}^+ f_{ip})(1 - \delta R_i + \delta R_i^2) + \sum_{i,j,p} t_{ij} r_o f_{ip}^+ f_{jp} + \sum_{i,j} V_{ij} r_o^2 \delta R_i \delta R_j - \mu \sum_{i,p} f_{ip}^+ f_{ip}(1 - \delta R_i + \delta R_i^2)$$

$$+ N r_0 \sum_i \delta\lambda_i \ \delta R_i + \sum_{i,p} f_{ip}^+ f_{ip}(1 - \delta R_i + \delta R_i^2) \ \delta\lambda_i - \sum_{ip} \mathcal{Z}_{ip}^\dagger (1 - \delta R_i + \delta R_i^2) \mathcal{Z}_{ip}, \quad (10)$$

where λ_0 has been absorbed in the chemical potential $\mu \to \mu - \lambda_0$ and all constant and linear terms in the fields have been dropped. The path-integral representation of $(\text{sdet} M_{AB})^{1/2}$, written in terms of the N-component boson ghost fields,[20] $\mathcal{Z}p$, leads to the last term of Lagrangian (10). Note that all the complications arising from the Hubbard algebra have been translated to an effective theory of fermions interacting with bosons. Indeed, the interaction terms appearing in the effective Lagrangian (10) are generated solely by the Hubbard algebra (apart from the no double-occupancy constraint) and are not present in the original Hamiltonian (3), which is quadratic in the Hubbard operators.

In the above expansion we have only retained the first nontrivial terms that couple the fermionic and bosonic modes. In order to have a systematic scheme to classify and

deal with these interaction terms we introduce a set of Feynman rules in powers of $1/N$.[19] These will help us to determine, for instance, that the terms retained in the effective Lagrangian (10) correspond to expanding through O(1/N) in the large-N expansion. The Feynman rules needed to carry out this project can be summarized as follows.

(i) *Propagators*. We associate with the two component $\delta X^a = (\delta R, \delta\lambda)$ boson field, the bare propagator D_0,

$$D_{(0)ab}^{-1}(\mathbf{q}, \nu_n) = N \begin{pmatrix} 4 V r_0^2 [\cos(q_x) + \cos(q_y)] & r_0 \\ r_0 & 0 \end{pmatrix},$$

$$(11)$$

which is represented by a dashed line in Fig. 1 connecting two generic components a and b. q and ν_n are the momentum and the Matsubara frequency of the boson fields, respectively.
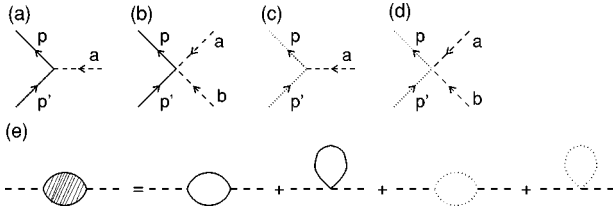
FIG. 1. Feynman diagrams in the large-N expansion of the Hubbard operator theory. Solid lines represent fermions which are related to the electrons. Dashed lines represent bosons which are related to charge fluctuations. Dotted lines represent ghosts which are not physical but related to the constraints appearing in the theory which enforce that fermions satisfy the Hubbard operator algebra. (a)–(d) The types of vertex which occur up to order O($1/N$). (a) The vertex between two fermions and one boson. (b) The vertex between two fermions and two bosons. (c) The vertex between two ghosts and one boson. (d) The vertex between two bosons and two ghosts. (e) The sum of all one-loop diagrams contributing to the irreducible boson self-energy which is of the order of O($1/N$).

The bare propagator of the N-component fermion field f_p reads

$$G_{(0)pp'}(\mathbf{k}, \omega_n) = -\frac{\delta_{pp'}}{i\omega_n - (\varepsilon_{\mathbf{k}} - \mu)}, \qquad (12)$$

which is represented by a solid line in Fig. 1 connecting two generic components p and p'. The electron dispersion relation appearing in Eq. (12) is the one associated with the original fermions renormalized by the interaction $\varepsilon_{\mathbf{k}} = -2tr_o[\cos(k_x) + \cos(k_y)]$, with t the hopping between nearest-neighbors sites on the square lattice. The quantities k and ω_n are the momentum and the fermionic Matsubara frequencies of the fermion field, respectively.

We associate with the N-component bare ghost field $\mathcal{Z}p$ the propagator

$$\mathcal{D}_{pp'} = -\delta_{pp'} \qquad (13)$$

which is represented by a dotted line in Fig. 1 connecting two generic components p and p'.

(ii) *Vertices.* The expressions of the different three-leg and four-leg vertices are

$$\Lambda_a^{pp'} = -\left(\frac{i}{2}(\omega + \omega') + \mu; \ 1\right)\delta^{pp'} \qquad (14)$$

representing the interaction between two fermions and one boson [see Fig. 1(a)];

$$\Lambda_{ab}^{pp'} = -\begin{pmatrix} -\frac{i}{2}(\omega + \omega') - \mu & -\frac{1}{2} \\ -\frac{1}{2} & 0 \end{pmatrix}\delta^{pp'} \qquad (15)$$

representing the interaction between two fermions and two bosons [see Fig. 1(b)];

$$\Gamma_{pp'}^a = (-1)(\delta_{pp'}, \ 0) \qquad (16)$$

representing the interaction between two ghosts and one boson [Fig. 1(c)]; and

$$\Gamma_{pp'}^{ab} = (-1)\begin{pmatrix} -1 & 0 \\ 0 & 0 \end{pmatrix}\delta_{pp'} \qquad (17)$$

representing the interaction between two bosons and two ghosts [Fig. 1(d)]. Each vertex conserves momentum and energy, as it should.

In the lowest order of the expansion $N = \infty$, we have the original fermions renormalized by the interaction $\varepsilon_{\mathbf{k}} = -2tr_o[\cos(k_x) + \cos(k_y)]$. For a given value of μ, r_0 must be determined self-consistently. For instance, r_0 is equal to $\delta/2$ (where δ is the hole doping away from half filling) from Eq. (8) and the completeness condition (4).

The path integral (5) is written in terms of the original X operators without having to introduce slave particles. Equation (5) is analogous to the path integral used for the Heisenberg model where, using SU(2) coherent states, the measure can be written[21] in terms of the spin $\vec{S}$. There is, however, an extra price we have to pay if we work with the original Hubbard operators. For instance, we need to introduce a new constraint [the second δ function in Eq. (5)] and the determinant (sdetM_{AB}) of the matrix formed by the constraints appearing in the theory.[19] In spite of these "apparent" complications our formulation is very flexible in calculating the physical quantities of interest, as it will be shown below.

In summary, we have developed a diagrammatic technique appropriate for a large-N expansion along the lines of the large-N expansion developed in quantum field theory. Hence, from the order of the propagators and vertices, we can determine the order of the diagram contribution.

To conclude this section we make contact with closely related approaches such as slave boson formulations. In contrast to slave boson theories, (a) Greens functions are calculated in terms of the original Hubbard operators, (b) fermions f_{ip} appearing in the theory are proportional to the Fermi-like X operator X^{op} [see Eq. (8)] to all orders in the $1/N$ expansion, not only to leading order,[22] (c) as our path integral is written in terms of X operators we do not need to introduce *a priori* any decoupling scheme, and (d) r_0 is the mean value of X^{00} which is a real field associated with the number of holes [see Eq. (8)] and not with the number of holons. At leading order [$N \to \infty$ or O(1)] and $V = 0$, our formalism is equivalent to slave boson approaches. However, at the next to leading order [O($1/N$)] [which is necessary to calculate one-electron properties such as the electron self-energy $\Sigma(\mathbf{k}, \omega)$ and the electron spectral function $A(\mathbf{k}, \omega)$], the two formulations do not coincide. The differences between the two formulations are not yet completely established. Our theory has the *significant advantage* that it does not require the introduction of gauge fields like in slave boson approaches. Hence, through order O($1/N$) we do not need to take care of gauge fluctuations or Bose condensation [note that Eq. (8) does not mean Bose condensation]. This is important because for the doped Hubbard model the gauge fluctuations are known to significantly change the physics.[23]

Careful numerical work will determine the improvements of the present approach with respect to slave boson formulations.

III. DYNAMICAL PROPERTIES OF THE METALLIC PHASE CLOSE TO THE CHARGE-ORDERING TRANSITION

In this section, we analyze using large-N and Lanczos techniques the influence of the charge-ordering transition on the dynamical properties of the normal metallic phase.

A. Charge response

The dynamical electronic density-density response function can be written in terms of Hubbard operators. We define the retarded density-density, Green's function as

$$\tilde{D}_{ij}(\tau) = \frac{1}{N} \sum_{pq} \langle T_\tau X_i^{pp}(\tau) X_j^{qq}(0) \rangle. \tag{18}$$

From $\sum_q X_i^{qq} = N/2 - X_i^{00}$ and Eq. (8) we find, after Fourier transforming,

$$\tilde{D}(\mathbf{q}, \nu_n) = -N \left(\frac{\delta}{2}\right)^2 D_{RR}(\mathbf{q}, \nu_n). \tag{19}$$

Here $D_{RR}(\mathbf{q}, \nu_n)$ is the (R,R) component of the boson propagator. This is the only physical component of the boson propagator and encodes the charge fluctuations occurring in the system. Other components of the boson propagator such as (λ, R) or (λ, λ) contain the nonphysical field λ which are introduced to enforce the no double-occupancy constraint. Unlike in slave boson theories, the (R,R) component used here is associated directly with the charge and not with a fictitious bosonic field (holon).

Through O($1/N$) the boson propagator consists of the bare boson propagator $D_{(0)}$ [which is of the order of O($1/N$)] renormalized by a random-phase-approximation (RPA)-type series of electronic bubbles. The irreducible boson self-energy components, Π_{ab}, are obtained (through order $1/N$) from the summation of all the contributions corresponding to the one-loop diagrams shown in Fig. 1(e).

The last two diagrams appearing in Fig. 1(e) involving ghost fields are very important. It is possible to show that these two diagrams exactly cancel the infinities, due to the frequency dependence of our vertices, of the two first diagrams appearing in Fig. 1(e). Ghost fields interact only with the boson fields as can be seen from Figs. 1(c) and 1(d). Summarizing, the only role of ghost fields, through order $1/N$, is to cancel infinities in the boson self-energy Π_{ab} arising from the frequency dependence of our vertices (14) and (15).

Using our Feynman rules, we can now write out explicitly each of the components of the boson self-energy Π_{ab},

$$\Pi_{RR}(\mathbf{q}, \nu_n) = -\frac{N}{N_s} \frac{1}{4} \sum_{\mathbf{k}} \left[2 \; n_F(\varepsilon_{\mathbf{k}} - \mu)(\varepsilon_{\mathbf{k}+\mathbf{q}} - \varepsilon_{\mathbf{k}}) \right.$$
$$\left. + (\varepsilon_{\mathbf{k}+\mathbf{q}} + \varepsilon_{\mathbf{k}})^2 \; \frac{[n_F(\varepsilon_{\mathbf{k}+\mathbf{q}} - \mu) - n_F(\varepsilon_{\mathbf{k}} - \mu)]}{-i\nu_n + \varepsilon_{\mathbf{k}+\mathbf{q}} - \varepsilon_{\mathbf{k}}} \right], \tag{20}$$

$$\Pi_{\lambda R}(\mathbf{q}, \nu_n) = -\frac{N}{N_s} \frac{1}{2} \sum_{\mathbf{k}} (\varepsilon_{\mathbf{k}+\mathbf{q}} + \varepsilon_{\mathbf{k}})$$
$$\times \frac{[n_F(\varepsilon_{\mathbf{k}+\mathbf{q}} - \mu) - n_F(\varepsilon_{\mathbf{k}} - \mu)]}{-i\nu_n + \varepsilon_{\mathbf{k}+\mathbf{q}} - \varepsilon_{\mathbf{k}}}, \tag{21}$$

and,

$$\Pi_{\lambda\lambda}(\mathbf{q}, \nu_n) = -\frac{N}{N_s} \sum_{\mathbf{k}} \frac{[n_F(\varepsilon_{\mathbf{k}+\mathbf{q}} - \mu) - n_F(\varepsilon_{\mathbf{k}} - \mu)]}{-i\nu_n + \varepsilon_{\mathbf{k}+\mathbf{q}} - \varepsilon_{\mathbf{k}}}, \tag{22}$$

where N_s is the number of sites of the system.

From Dyson's equation and Π_{ab} the dressed components of the boson propagator, D_{ab}, can be found:

$$(D_{ab})^{-1} = (D_{(0)ab})^{-1} - \Pi_{ab}. \tag{23}$$

D_{ab} may contain collective excitations such as zero sound.[22]

In order to look at charge-ordering instabilities induced by the intersite Coulomb interaction, V, we have calculated the static charge susceptibility $\tilde{D}(\mathbf{q}, \nu_n = 0)$ for different $\mathbf{q}$ vectors on the Brillouin zone (BZ). At one-quarter filling ($\delta = 0.5$) the corresponding chemical potential is $\mu = -0.360t$ in the limit $N \to \infty$. We find that the static susceptibility diverges at the wave vector $\mathbf{q_c} = (\pi, \pi)$ for $V = V_c \approx 0.65t$ signaling the instability to a checkerboard charge-density wave. The value of V_c is slightly smaller than the one previously found using slave bosons,[4] $V_c \approx 0.69t$. This is because of the decoupling of the electron operators introduced within slave bosons to treat the intersite interaction term $V n_i n_j$ which is not needed (due to the use of Hubbard operators) in the present large-N approach. For comparison, recent exact diagonalization calculations[11] give a critical value for the metal-insulator transition driven by V at about $V_c \approx 2t$ for $U = 20t$. The large difference in V_c between large-N and Lanczos diagonalization calculations can be attributed to the strong renormalization of the bare band (given by $r_0 = \delta/2$) which appears in large-N approaches at O(1). Our comparison to Lanczos will show that in spite of the difference in the absolute magnitude of V_c, dynamical properties computed from the $1/N$ expansion are in rather good agreement as $V \to V_c$, making the $1/N$ approach reliable.

In Fig. 2 we show the evolution of $-\text{Im}\,\tilde{D}(\mathbf{q_c}, \nu)$ as the system is driven close to the charge-ordering instability, $V < V_c$, for the wave vector: $\mathbf{q_c} = (\pi, \pi)$. The intersite Coulomb repulsion softens the collective mode at $\mathbf{q_c}$ which appears for $U \to \infty$ and $V = 0$ and, at the same time, increases its weight. At wave vectors far from $\mathbf{q_c}$ the collective mode shows up as a peak located at frequencies of about t which carries small weight and is barely influenced by V. The mode at (π, π) can be detected, in principle, with electron energy-
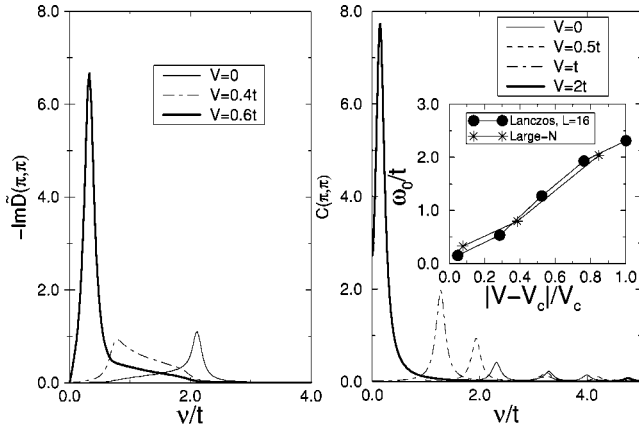
FIG. 2. The softening of the collective mode at the wave vector $\mathbf{q_c}=(\pi,\pi)$ as the system is driven closer to the checkerboard charge-ordering transition. The frequency dependence of the charge correlation function is shown for several different values of V/t. The right and left panels show results obtained using Lanczos diagonalization on $L=16$ site clusters ($U=20t$) and large-N theory, respectively. A Lorentzian broadening of $\eta=0.1t$ is used in the calculations. Only for wave vectors close to or at (π,π), the softening of the collective mode is observed as a consequence of the proximity of the system to a checkerboard charge-ordering transition. Calculations of dynamical properties using large-N theory at O($1/N$), which couples the electrons to the short-range charge fluctuations associated with this transition, and Lanczos diagonalization, suggest that this collective mode is responsible for the "unconventional" behavior of dynamical properties. The inset compares the position of the peak associated with the collective mode at (π,π) computed from Lanczos and large-N approaches.

loss scattering (EELS) (Ref. 24) or inelastic x-ray scattering.[25] With EELS one is able to obtain information on the electronic properties of the system at a given energy and wave vector, so that, for instance, the dispersion relation of the mode can be mapped out. A more appropriate way of detecting this mode is by using inelastic x-ray scattering, which provides a direct probe of the dynamical charge correlation function and has been successfully applied to one- and two-dimensional Mott-Hubbard systems.[25]

In order to compare with large-N we compute, with Lanczos diagonalization, the spectral decomposition of the charge correlation function,

$$C(\mathbf{q},\nu)=\sum_m |\langle m|N_{\mathbf{q}}|0\rangle|^2 \delta[\nu-(E_m-E_0)], \qquad (24)$$

where $N_{\mathbf{q}}=1/\sqrt{L}\sum_i e^{i\mathbf{q}\mathbf{R_i}}(c_i^+ c_i - \langle c_i^+ c_i \rangle)$. E_m and E_0 denote the excited- and ground-state energies of the system, respectively. L is the number of sites in the cluster. Note that $C(\mathbf{q},\nu)$ can be compared to $-\operatorname{Im}\tilde{D}(\mathbf{q_c},\nu)$ as they have equivalent definitions. Of course, attention must be paid to the fact that we are comparing calculations of the charge susceptibility on an infinite system with calculations on an $L=16$ cluster. Indeed, we find that $C(\mathbf{q_c},\nu)$ is in rather good agreement with $-\operatorname{Im}\tilde{D}(\mathbf{q_c},\nu)$ (see Fig. 2), both displaying similar softening and increase in amplitude of the collective mode at (π,π) close to the charge-ordering transition.
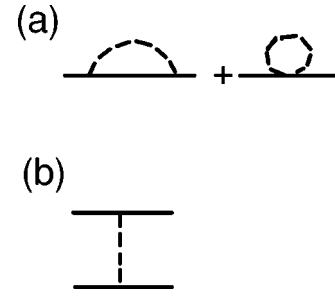

FIG. 3. (a) Contributions to the electron self-energy, $\Sigma(\mathbf{k},\omega)$, through O($1/N$), in the Hubbard operator theory. The first diagram contains two three-leg vertices as the ones shown in Fig. 1(a) and the second one is formed with one four-leg vertex as shown in Fig. 1(b). (b) Contribution to the effective interaction between quasiparticles, V_{eff}, through O($1/N$). This interaction is used in the present work to analyze superconducting instabilities of the Fermi liquid induced by the charge fluctuations appearing close to a checkerboard charge-ordering transition induced by V.

The imaginary part of the charge correlation close to the charge-ordering wave vector $\mathbf{q}\to\mathbf{q_c}$ can be fitted to the following RPA form:[26]

$$-\operatorname{Im}\tilde{D}(\mathbf{q},\nu)=A\frac{\nu}{\nu^2+\omega_{\mathbf{q}}^2}, \qquad (25)$$

where $\omega_{\mathbf{q}}=\omega_0+C(\mathbf{q}-\mathbf{q_c})^2$, where A and C are constants. ω_0 gives the position of the peak appearing in the charge correlation function at (π,π) for different V's and goes to zero as $V\to V_c$, measuring the proximity of the system to the charge-ordering transition (see inset of Fig. 2). We note that the overall behavior of the charge susceptibility is analogous to the one of the spin susceptibility in nearly antiferromagnetic metals.[27,28]

B. Spectral densities

The Green's function Eq. (12) corresponds to the N-infinite propagator which is just proportional to the Hubbard operators, $X^{0\sigma}$ [see Eq. (12)]. In spite of involving the many-body Hubbard operators Eq. (12) looks similar to the propagator for free electrons although its physical interpretation is very different. Equation (12) describes quasiparticles with renormalized hopping $t(k)\delta/2$. The $N=\infty$ propagator in Eq. (12) does not contain dynamical corrections; these appear at higher orders in the $1/N$ expansion. In order to calculate spectral densities, we first calculate the self-energy. Using the Feynman rules, there are two diagrams, shown in Fig. 3(a), contributing to the self-energy through O($1/N$). The analytical expression for these two diagrams reads

$$\Sigma_{pp}=\sum_{p',p'',a,b} \Lambda_a^{pp'} D_{ab} G_{p'p''}\Lambda_b^{p''p}+\sum_{a,b} \Lambda_{ab}^{pp}D_{ab}, \quad (26)$$

where integration over internal momenta and sum over Matsubara frequencies is assumed. The renormalized boson propagator in Eq. (23) plays a similar role as the phonon propagator when dealing with the electron-phonon interaction in simple metals. Therefore, in the calculation of
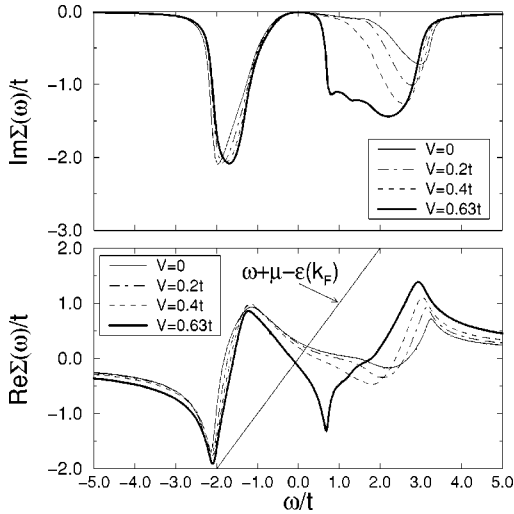
FIG. 4. Evolution of the real and imaginary parts of the self-energy of an electron at the Fermi surface as the system is driven close to the checkerboard charge-ordering transition from large-N theory. The amplitude of the self-energy is enhanced at frequencies between t and $3t$ due to the enhancement of fluctuations associated with (π,π) short-range charge ordering. The behavior of the self-energy leads to an enhancement of spectral weight in the spectral density (see Fig. 5) and an incoherent band in the density of states (DOS) (see Fig. 8) between $\omega=t$ and $3t$ as we approach the charge-ordering transition. The intersection of the curve of $\mathrm{Re}\,\Sigma(\omega)$ vs ω with $\omega+\mu-\epsilon(\mathbf{k})$ determines the quasiparticle peaks in the electronic spectral function.

$\Sigma(k,\omega)$ through $\mathrm{O}(1/N)$ not only band-structure effects enter, but also collective effects associated with the charge degrees of freedom (this self-energy calculation is analogous to the large-N expansion within slave boson formulations[22]).

Using the spectral representation for the boson fields, D_{ab}, the imaginary part of the self-energy $\mathrm{Im}\,\Sigma$ can be obtained,

$$\mathrm{Im}\,\Sigma(\mathbf{k},\omega)=-\frac{1}{N_s}\sum_{\mathbf{q}}\left\{\frac{1}{4}\mathrm{Im}\left[D_{RR}(\mathbf{q},\omega-\varepsilon_{\mathbf{k}-\mathbf{q}})\right]\right.$$

$$\times(\varepsilon_{k-q}+2\mu+\omega)^2+\mathrm{Im}\left[D_{R\lambda}(\mathbf{q},\omega-\varepsilon_{\mathbf{k}-\mathbf{q}})\right]$$

$$\times(\varepsilon_{\mathbf{k}-\mathbf{q}}+2\mu+\omega)+\mathrm{Im}\left[D_{\lambda\lambda}(\mathbf{q},\omega-\varepsilon_{\mathbf{k}-\mathbf{q}})\right]\Big\}$$

$$\times(n_B(\omega-\varepsilon_{\mathbf{k}-\mathbf{q}})+n_F[-\varepsilon_{\mathbf{k}-\mathbf{q}}]). \qquad (27)$$

Note that this self-energy is the one associated with the propagator $G(\mathbf{k},\omega)$ of the f operators.

Figure 4 shows the behavior of $\mathrm{Im}\,\Sigma(\mathbf{k},\omega)$ with increasing V for a wave vector on the Fermi surface: $\mathbf{k}=(1.204,1.204)$ (we have used $\eta=0.1t$ in the analytical continuation). As we approach $V=V_c$, both the imaginary and real parts of the self-energy [which from Eq. (27) involves a sum over the full BZ] are enhanced in the positive range of frequencies $t-3t$ due to the scattering of the electrons off the checkerboard charge fluctuations. Performing a Kramers-Kronig transformation on $\mathrm{Im}\,\Sigma$, we can obtain the real part

of the self-energy, $\mathrm{Re}\,\Sigma$, which is also plotted in Fig. 4. It is worth noting that for $U=\infty$ and $V=0$ the self-energy is already nonzero as a consequence of the interaction of fermions with the collective mode present in the charge correlation function.

From $\mathrm{Im}\,\Sigma(\mathbf{k},\omega)$ and $\mathrm{Re}\,\Sigma(\mathbf{k},\omega)$, we can compute the spectral function $A(\mathbf{k},\omega)=-(1/\pi)\mathrm{Im}\,G(\mathbf{k},\omega)$ as

$$A(\mathbf{k},\omega)=-\frac{1}{\pi}\frac{\mathrm{Im}\,\Sigma(\mathbf{k},\omega)}{(\omega+\mu-\varepsilon_{\mathbf{k}}-\mathrm{Re}\,\Sigma(\mathbf{k},\omega))^2+\mathrm{Im}\,\Sigma(\mathbf{k},\omega)^2}. \qquad (28)$$

The spectral density $A(\mathbf{k},\omega)$ calculated and plotted in Fig. 5 is associated with the f operators. As these anticommute, $A(\mathbf{k},\omega)$ integrates to 1. For the physical Hubbard operators as defined from the change of variables expressed in Eq. 9, the total spectral weight would sum to $N\delta/2$, which is the correct sum rule in the $N\to\infty$ limit. Deviations appear as N is made finite. For instance, for $N=2$ the total spectral weight of the Hubbard operators would give δ instead of $(1+\delta)/2$, so that 66.66% of the full sum rule would be captured at one-quarter filling. Similar deviations in the sum rule are found in related slave boson approaches[29] in the $N\to\infty$ limit. In the present approach we have expanded the self-energy to $\mathrm{O}(1/N)$ and computed Green's function of the f operators. An alternative route would have been to expand directly the propagators to $\mathrm{O}(1/N)$. In this way one could see how the $\mathrm{O}(1/N)$ fluctuations restore part of the sum rule.

In Fig. 5 we show the spectral function obtained from large-N theory, for an electron at $\mathbf{k}=(0,0),(1.204,1.204),(\pi,\pi)$ for different values of $V\to V_c$. The spectral density of an electron at the Fermi surface displays a quasiparticle peak characteristic of a Fermi liquid at $\omega=\mu$. The rest of spectral weight that is left is incoherent.

The quasiparticle weight $Z_{\mathbf{k}}$ evaluated at the Fermi surface is defined as

$$Z_{\mathbf{k}}=\left(1-\frac{\partial\mathrm{Re}\,\Sigma(\mathbf{k},\omega)}{\partial\omega}\right)^{-1}\Bigg|_{\omega=0}. \qquad (29)$$

In the inset of Fig. 5 we observe how a gradual suppression of $Z_{\mathbf{k}}$ occurs as the charge-ordering transition is approached. This can be compared to the suppression of the Drude weight found in Lanczos calculations,[11] which is also evident in the spectral function plotted in Figs. 6 and 7. Spectral weight is transferred from the quasiparticle peak to the range of energies between t and $3t$, as V tends to V_c due to the scattering of the electrons off the charge fluctuations associated with short-range checkerboard charge ordering. The modes close to (π,π) give the strongest contribution to the scattering. The apparent peak around $\omega=-2t$ should not be interpreted as a quasiparticle peak but as the lower Hubbard band[29] associated with the on-site Coulomb repulsion U.

The behavior of the spectral density shown in Fig. 5 can be now understood from the evolution of the real part of the self-energy shown in Fig. 4. The scattering of electrons from the strong charge fluctuations at (π,π) wave vectors in-
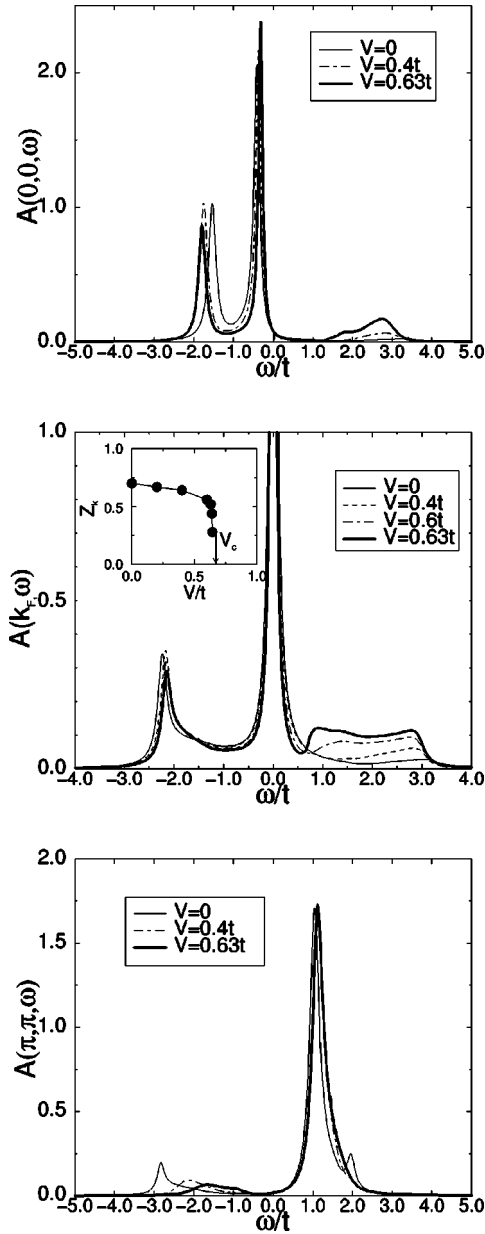
FIG. 5. Evolution of quasiparticle spectral density of states associated with the *f*-operator propagator computed from large-*N* theory at different wave vectors $\mathbf{k}=(0,0)$, (k_F,k_F), and (π,π). Close to the charge-ordering transition spectral weight is transferred from the quasiparticle peak to low and intermediate frequencies. The quasiparticle weight at the Fermi energy, $Z_\mathbf{k}$, is rapidly suppressed (see inset) as the charge-ordering transition is approached, $V \to V_c$. The results presented here can be compared with $A(\mathbf{k},\omega)$ computed from Lanczos calculations shown in Figs. 6 and 7.

volves large frequencies. This leads to an enhancement of the real part of the self-energy at large frequencies which, in turn, produces an increase of spectral weight at large and intermediate energies. This behavior is analogous to the one found in metals in the presence of short-range spin fluctuations.[30] Unlike in the case of nearly antiferromagnetic metals, no new poles induced by the interaction arise. This is because at quarter filling no two points of the Fermi surface are connected by the scattering wave vector $\mathbf{q}_c=(\pi,\pi)$, and
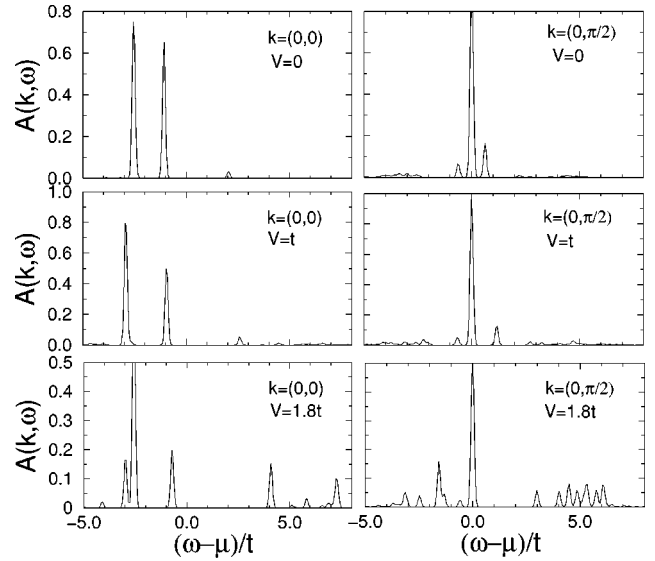

FIG. 6. Evolution of quasiparticle spectral density of states, $A(\mathbf{k},\omega)$, at $\mathbf{k}=(0,0)$ and $(0,\pi/2)$, computed from Lanczos diagonalization on an $L=16$ cluster for an extended Hubbard model at quarter filling. The on-site Coulomb repulsion is taken to be $U=20t$ and a broadening of the δ peaks, $\eta=0.1t$, is used. As the system approaches the metal-insulator transition, an enhancement of spectral weight at finite frequencies and a suppression of the weight at the Fermi energy takes place. At $\mathbf{k}=(0,0)$, the two sharp peaks are associated with the lower Hubbard band and the quasiparticle peak. An overall qualitative agreement with the results from large-*N* theory is found (see Fig. 5).

therefore the effect of the fluctuations near $\mathbf{q}_c$ on the electrons is weaker than spin fluctuations in systems close to half filling.

In order to test the validity of the large-*N* approach we have also computed the spectral densities from Lanczos diagonalization of finite clusters,[31]

$$A^{(+)}(\mathbf{k},\omega)=\sum_m |\langle m,N_e+1|c_{\mathbf{k}\sigma}^+|0,N_e\rangle|^2$$
$$\times \delta\{\omega-[E_m(N_e+1)-E_0(N_e)]\} \quad (30)$$

for adding and electron to the system with N_e electrons and

$$A^{(-)}(\mathbf{k},\omega)=\sum_m |\langle m,N_e-1|c_{\mathbf{k}\sigma}|0,N_e\rangle|^2$$
$$\times \delta\{\omega+[E_m(N_e-1)-E_0(N_e)]\} \quad (31)$$

for removing an electron from the N_e electron system. E_m and E_0 denote the excited- and ground-state energies of the system and $c_{\mathbf{k}\sigma}^\dagger=1/\sqrt{L}\sum_j e^{i\mathbf{k}\mathbf{R}_j}c_{j\sigma}^\dagger$.

In Figs. 6 and 7 we plot the evolution of the spectral densities calculated with Lanczos techniques for wave vectors at $\mathbf{k}=(0,0),(\pi/2,0),(\pi/2,\pi/2)$, and (π,π) for different values of V/t. At $\mathbf{k}=(0,0)$ two sharp peaks are clearly distinguished already for $V=0$. One of them is the quasiparticle peak and we associate the lower one with the lower Hubbard band due to the presence of U. For the nearest wave vectors to the Fermi energy, $\mathbf{k}=(\pi/2,0)$ and $(\pi/2,\pi/2)$, we find an
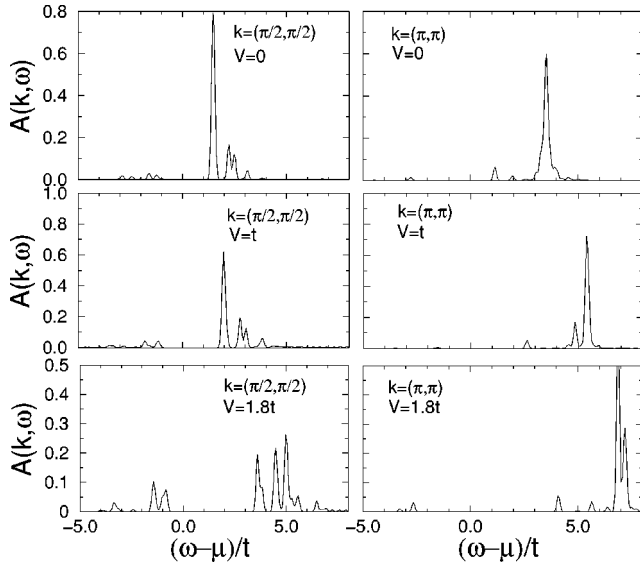
FIG. 7. Evolution of quasiparticle spectral density of states, $A(\mathbf{k},\omega)$, at $\mathbf{k}=(\pi/2,\pi/2)$ and (π,π), computed from Lanczos diagonalization on an $L=16$ site cluster for an extended Hubbard model at quarter filling. The on-site Coulomb repulsion is taken to be $U=20t$ and a Lorentzian broadening of the delta peaks, $\eta=0.1t$, is used.

enhancement of incoherent spectral weight at finite frequencies as the charge-ordering transition is approached.

Finally, the total density of states (DOS) can be computed from

$$N(\omega)=\frac{1}{L}\sum_{\mathbf{k}}\ [A^{(-)}(\mathbf{k},\omega)+A^{(+)}(\mathbf{k},\omega)]. \qquad (32)$$

In Fig. 8 we compare the evolution of the DOS, $N(\omega)$, for increasing V/t, calculated with both Lanczos at $U\to\infty$ and large-N calculations.

From Lanczos calculations we observe (left panel of Fig. 8) for $V=0$ a band at about $-3t$, a quasiparticle band situated at $\omega=\mu$, and a band running from t to $5t$. As V/t is increased the weight of the quasiparticle peak is reduced and weight between $2t$ and $5t$ is gradually enhanced. Also a suppression of spectral weight at low frequencies occurs as a precursor effect before the charge-ordering transition takes place. This general behavior is in qualitative agreement with large-N calculations. Indeed, an incoherent band at negative frequencies of about $-2t$, associated with the lower Hubbard band, a suppression of states close to the Fermi energy, and an overall enhancement of spectra between t and $3t$ occurs (see right panel of Fig. 8). However, we note that the pseudogap appearing within large-N is less pronounced than in Lanczos calculations. This can be attributed to finite-size effects appearing in small cluster Lanczos calculations.

C. Optical conductivity

It is interesting to analyze the behavior of the optical conductivity as the system is driven through the charge-ordering transition. Using Lanczos diagonalization we have computed
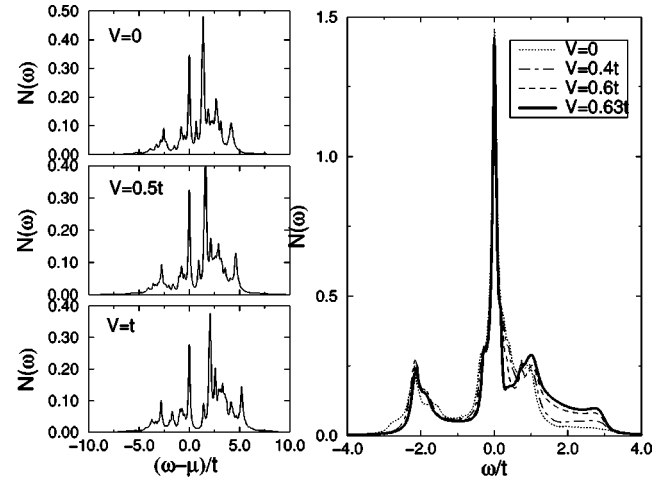

FIG. 8. Evolution of the DOS as the charge-ordering transition is approached from the metallic phase. The left and right panels show results from exact diagonalization on a 16-site lattice with $U\to\infty$ and large-N approaches, respectively. (The critical value of V is $V_c\approx 2t$ and $0.65t$, respectively.) A Lorentzian broadening of $\eta=0.1t$ has been introduced in the exact diagonalization calculations, to aid comparison with the large-N results. As the intersite Coulomb repulsion V is increased, the density of states close to the Fermi energy is gradually suppressed indicating the proximity to the charge-ordering transition. At the same time spectral weight is enhanced for frequencies in the range $t-3t$ in the large-N calculations. The peak at $-2t$ is an incoherent band associated with the lower Hubbard band. An overall qualitative agreement between Lanczos and large-N calculations is found.

$$\sigma(\omega)=D\,\delta(\omega)+\frac{\pi e^2}{L}\sum_{n\neq 0}\frac{|\langle n|j_x|0\rangle|^2}{E_n-E_0}\delta(\omega-E_n+E_0), \qquad (33)$$

where j_x is the current in the x direction, E_0 the ground-state energy and E_n the excited-state energies of the system, e is the electron charge, and the Drude weight is denoted by D.

The following sum rule[32] is satisfied by $\sigma(\omega)$:

$$\int_0^{\infty}\sigma(\omega)d\omega=-\frac{\pi e^2}{4L}\langle 0|T|0\rangle. \qquad (34)$$

where T is the kinetic-energy operator, which is the first term in the Hamiltonian (1).

The optical conductivity is plotted in Fig. 9, for increasing values of the ratio V/t and fixed $U=20t$. At $V=0$ we find a Drude peak and a broad mid-infrared band centered at about $3t$. As V/t is increased the mid-infrared band is enhanced and a well-defined feature builds up at the lower edge of the mid-infrared band, at frequencies of about $2t$. Also an incoherent band present at larger energies of the order of U (not shown for clarity) is gradually suppressed and its associated weight transferred to the mid-infrared band as V is increased. From the behavior of spectral densities and DOS shown in Figs. 5–8, we attribute the enhancement of optical weight observed in the mid-infrared range to an increase in the incoherent excitations carried by each quasiparticle as a result of charge fluctuations associated with short-range checkerboard charge ordering. From the behavior of the spectral
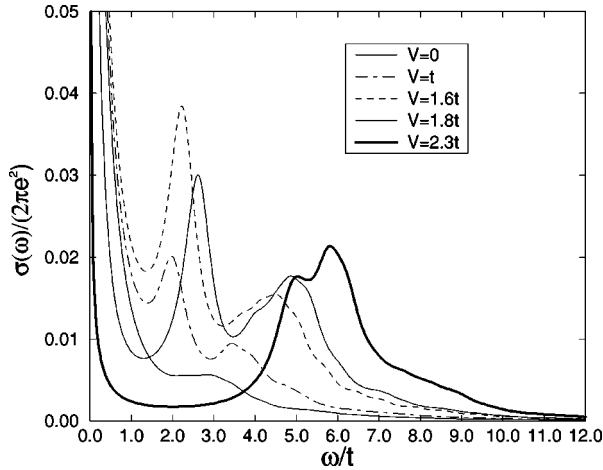
FIG. 9. Evolution of the optical conductivity computed from Lanczos diagonalization as the system is driven through the metal-insulator transition. The calculation is performed on an $L=16$ site cluster, $U=20t$, and different V, with a Lorentzian broadening of $\eta=0.4t$. Enhancement of optical weight at low frequencies is found as V is increased. The broad band situated at about $3V$ (for large V/t) is due to incoherent transitions between different sites induced by the intersite Coulomb repulsion. We interpret the low-energy feature appearing at about $2t$ as a consequence of transitions between the incoherent band and the quasiparticle peak found in the spectral densities $A(\mathbf{k},\omega)$ for wave vectors on the Fermi surface.

densities $A(\mathbf{k},\omega)$ shown in Figs. 6 and 7 and assuming that a lowest-order diagram (neglecting vertex corrections) is enough to compute the optical conductivity we would attribute the low-energy feature to transitions between the incoherent band carried by each quasiparticle and the quasiparticle peak situated at the Fermi energy. This interpretation is plausible if one notes that the low-energy feature observed in Fig. 9 moves together with the broadband as V/t is increased. Similar results would be obtained from large-N theory evaluating the bubble Feynman diagram for the optical conductivity, as the spectral densities obtained are similar to the ones obtained from Lanczos diagonalization.

IV. CONNECTION TO EXPERIMENTAL RESULTS

Recent experiments with Raman scattering[33] and optical conductivity measurements[34] on the insulating salt θ-(BDT-TTP)$_2$Cu(NCS)$_2$ find that the checkerboard charge-ordered state discussed in this paper is indeed the ground state. This gives experimental support to the model discussed here. A discussion of other possible orderings within more complicated models can be found in the work by Seo[35] and Clay, Mazumdar, and Campbell.[36]

We review now the experiments on resistivity measurements on several quarter-filled organics, and make contact with the predictions of the large-N approach presented.

From the imaginary part of the self-energy [Eq. (27)] we can obtain the behavior of the inverse of the lifetime of the quasiparticles, $1/\tau(T)=-2\operatorname{Im}\Sigma(k_F,0)$ with temperature as shown in Fig. 10. From this plot we obtain a temperature scale, $T^*\approx0.22t$, at which $1/\tau(T)$ changes from T^2 to T
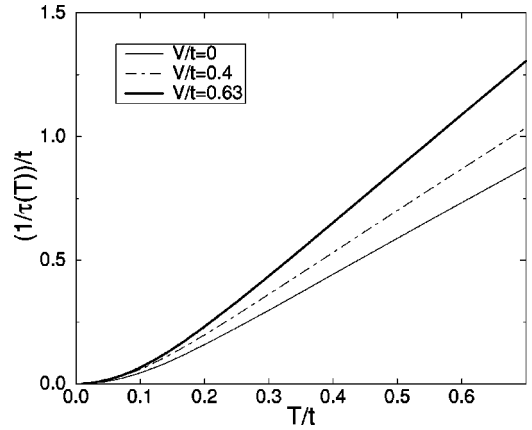

FIG. 10. Temperature dependence of the scattering rate $1/\tau(T)=-2\operatorname{Im}\Sigma(\mathbf{k_F},\omega=0)$. This scattering, which is due to charge fluctuations, increases as the charge-ordering transition is approached. As the temperature increases above about $T^*\approx0.22t$, $1/\tau(T)$ changes from a T^2 dependence to a linear behavior in T. This temperature scale depends only slightly on V, so that large-N theory [through $O(1/N)$] predicts Fermi-liquid behavior close to the charge-ordering transition at temperatures below T^*.

behavior. The temperature scale defined by T^* decreases only slightly as we approach the charge-ordering transition remaining finite as $V \to V_c$ (through $O(1/N)$). This is in contrast to dynamical mean-field approaches where a similar low-temperature scale is suppressed as the Mott-Hubbard metal insulator (driven by U instead of V) is approached.[37] Hence, Fermi-liquid behavior is found below this temperature scale even close to the charge-ordering transition occurring at $V \approx V_c$. Presumably, higher-order corrections in the $1/N$ expansion may suppress the region where the system behaves as a Fermi liquid as $V \to V_c$. Future work should focus in understanding this issue better.

We have also computed the temperature dependence of the effective mass defined as $m^*/m=1/Z_k(T)$, evaluated at the Fermi surface, and is shown in Fig. 11. Large-N theory predicts an increase of m^*/m as the temperature is raised for $V \to V_c$. This means that the system becomes more incoherent as the temperature is increased. Interestingly this behavior is also found in the Hubbard model in the limit of infinite dimensions close to the Mott metal-insulator transition.[38] However in that case the system is close to a metal-insulator transition which takes place between two nonordered phases, in contrast to the charge-ordering transition discussed here. At $V=0$ the effective mass is temperature independent as one would expect from a weakly interacting system. At the lowest temperatures we obtain enhanced effective masses in the range 1.3–2 for V/t varying from 0 to 0.63.

In Fig. 12 we show optical conductivity data of θ-(BEDT-TTF)$_2$CsCo(SCN)$_4$ along the a direction[39] at $T=15$ K. This salt is metallic down to temperatures of about 10 K. At this temperature a charge-ordering transition to an insulating phase takes place. The observed optical conductivity displays a band situated at 1.2 eV, a mid-infrared band appearing at frequencies of about 0.25 eV, and a feature appearing at low frequencies of about 0.13 eV. In the same figure we present a comparison of our exact diagonalization
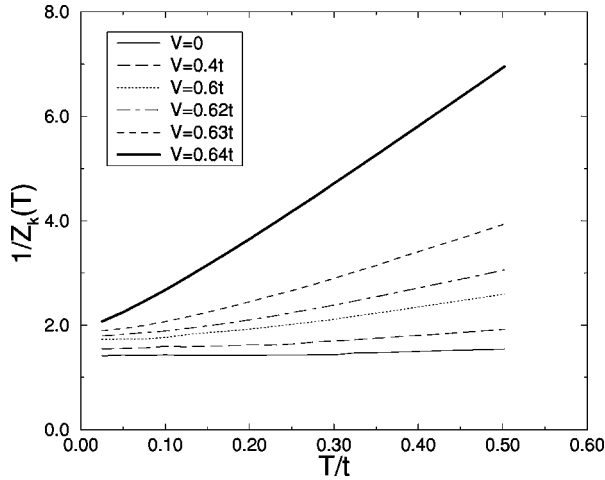
FIG. 11. Temperature dependence of the effective mass of an electron on the Fermi surface, $m^*/m \equiv 1/Z_k(T)$, as obtained from large-N theory through O($1/N$). As the system is driven closer to the charge-ordering transition a stronger increase of the effective mass with T is found.

calculations of the optical conductivity performed on a 16-site cluster, $U/t = 20$ and $V/t = 1.2$, where we have set the hopping energy scale to $t = 0.061$ eV, so that we associate the mid-infrared band observed experimentally with the one from exact diagonalization calculations. In this way, we recover the main features appearing in the experimental data, including the incoherent high-frequency feature and the fea-
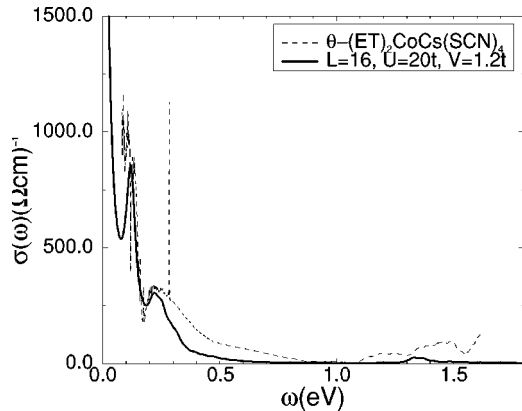

FIG. 12. Comparison of the optical conductivity computed from Lanczos diagonalization on $L = 16$ site clusters with experimental results (Ref. 39) for the metallic salt θ-(BEDT-TTF)$_2$CsCo(SCN)$_4$. For the exact diagonalization results we have chosen $U = 20t$ and $V = 1.2t$. In order to fit the data we chose $t = 0.061$ eV, which can be compared to values from Hückel band-structure calculations (Ref. 40). The lattice parameters for θ-(BEDT-TTF)$_2$CsCo(SCN)$_4$ are $a = 9.804$ Å, $c = 4.873$ Å, and $V_{cell} = 4V_{mol} = 2074$ Å^3, where V_{cell} and V_{mol} are the volumes per unit cell and per molecule, respectively. The broadband at about 0.25 eV and the low-energy feature at 0.13 eV can be explained from short-range charge ordering induced by the intersite Coulomb repulsion V. This behavior is characteristic of several quarter-filled layered metallic salts which undergo a metal-insulator transition at sufficiently low temperatures.
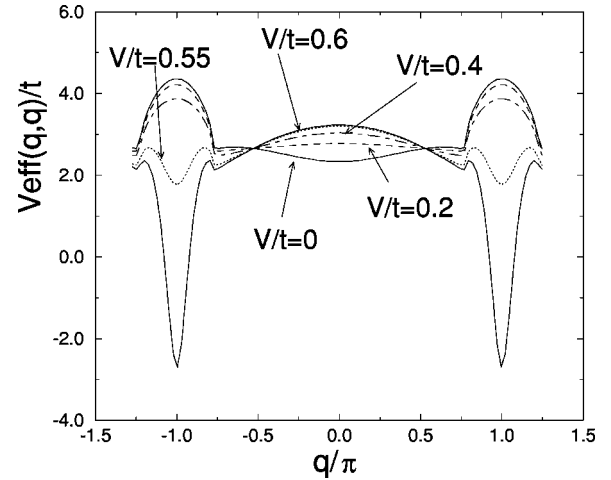

FIG. 13. Behavior of the effective potential between quasiparticles, $V_{eff}(q_x, q_y)$, as a function of momenta for increasing V/t values along the $q_x = q_y = q$ direction. As $V/t \rightarrow (V/t)_c$, the effective potential becomes negative at the (π, π) points, becoming singular at the transition to the checkerboard charge-ordered insulator. It is the momentum dependence of the potential shown here which leads to the d_{xy} symmetry of the Cooper pairs. This calculation was done using the large-N approach through O($1/N$).

ture appearing at low frequencies. This behavior is commonly observed in metallic θ-salts close to the metal-insulator transition[11] and from Fig. 12 we note that the low-energy feature can be misinterpreted as being part of the Drude peak. Caution is in order when comparing our results with experimental data as shown in Fig. 12 because some features such as the dip appearing at about 0.17 eV have been interpreted in θ-(ET)$_2$RbZn(SCN)$_4$ (where a structural transition takes place with lowering temperature) as being caused by the coupling to vibronic modes of the ET molecules.[39] More experimental and theoretical work is needed to understand this issue better.

V. SUPERCONDUCTIVITY

In the present section we discuss the possibility of having superconductivity close to the charge-ordering transition induced by the short-range charge fluctuations which appear in the metallic phase. Here we extend the discussion presented in Ref. 6 and provide full details of the calculations. We also consider the binding energy of holes using a Lanczos calculation.

A. Large N: Pairing symmetry

Within the large-N approach, superconductivity is possible at O($1/N$). As we have already seen at O(1), our approach describes quasiparticle excitations with renormalized masses. Interaction between these quasiparticles can appear at the next-to-leading order of O($1/N$). The effective interaction between electrons are those represented diagrammatically in Fig. 3(b); only the three-leg vertex shown in Fig. 1(a) contributes to the effective interaction through order O($1/N$).

Using the Feynman rules introduced above [see Fig. 3(b)], the interaction between the quasiparticles $\Theta(\mathbf{k},\mathbf{k}')$ reads

$$\Theta(\mathbf{k}-\mathbf{k}',\omega_n-\omega_{n'}) = -[\mu^2 D_{RR}(\mathbf{k}-\mathbf{k}',\omega_n-\omega_{n'})$$
$$+2\mu D_{R\lambda}(\mathbf{k}-\mathbf{k}',\omega_n-\omega_{n'})$$
$$+D_{\lambda\lambda}(\mathbf{k}-\mathbf{k}',\omega_n-\omega_{n'})], \quad (35)$$

where μ is the chemical potential and D_{ab} are the components of the boson propagator which are obtained from Dyson's equation (23).

In Fig. 13 we plot the dependence of $V_{eff}(\mathbf{q}=\mathbf{k}-\mathbf{k}') \equiv \Theta(\mathbf{q},\omega\rightarrow 0)/(\delta/2)$, that is, the static limit of the effective interaction mediating the possible pairing between the quasiparticles. This clearly shows the development of the singularity due to checkerboard charge ordering at the (π,π) wave vectors. We note that the effective interaction Θ obtained from Eq. (35), which is valid on the whole Brillouin zone, coincides only with the one obtained using slave boson approaches, when it is evaluated at the Fermi surface.[17] This is not true for wave vectors outside the Fermi surface.

In weak coupling, we use this effective potential to compute the effective couplings in the different pairing channels or irreducible representations of the order parameter, i [$i = (d_{x^2-y^2}, d_{xy}, s)$]. In this way we project out the interaction with a certain symmetry. The critical temperature T_c can then be estimated from $T_{ci} = 1.13\omega_0 \exp(-1/|\lambda_i|)$, where ω_0 is a suitable cutoff frequency and λ_i are the effective couplings with different symmetries. These are defined as:[17,41]

$$\lambda_i = \frac{1}{(2\pi)^2} \frac{\int (d\mathbf{k}/|v_\mathbf{k}|) \int (d\mathbf{k}'/|v_{\mathbf{k}'}|) g_i(\mathbf{k}') V_{eff}(\mathbf{k}'-\mathbf{k}) g_i(\mathbf{k})}{\int (d\mathbf{k}/|v_\mathbf{k}|) g_i(\mathbf{k})^2}, \quad (36)$$

where the functions $g_i(\mathbf{k})$ encode the different pairing symmetries, and $v_\mathbf{k}$ are the quasiparticle velocities at the Fermi surface. The integrations are restricted to the Fermi surface. λ_i measures the strength of the interaction between electrons at the Fermi surface in a given symmetry channel i. If $\lambda_i > 0$, electrons are repelled. Hence, superconductivity is only possible when $\lambda_i < 0$. In Fig. 14 we plot the dependence of the effective couplings in the possible symmetry channels with V/t.

We observe that near the charge-ordering instability, but still in the metallic phase $V < V_c$, the coupling in the d_{xy} channel, $\lambda_{d_{xy}}$, becomes attractive whereas other couplings become more repulsive. However, we note that the couplings are rather small. This implies that critical temperatures are expected to be small. Similar conclusions have been reached with large-N treatments of the U-infinite Hubbard model at $V=0$ close to half filling.[42] Exact diagonalization results also
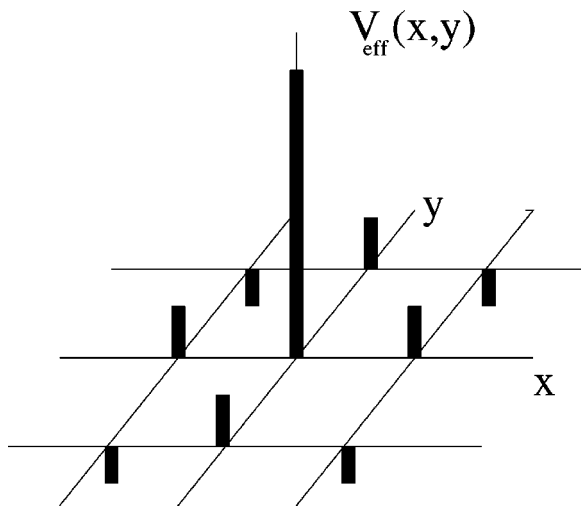
FIG. 14. Dependence of the effective couplings with V/t as defined in Eq. (36) in the different symmetry channels. Close to the charge-ordering transition pairing in the d_{xy} channel becomes favorable while other possible pairing symmetries are repulsive for any V.
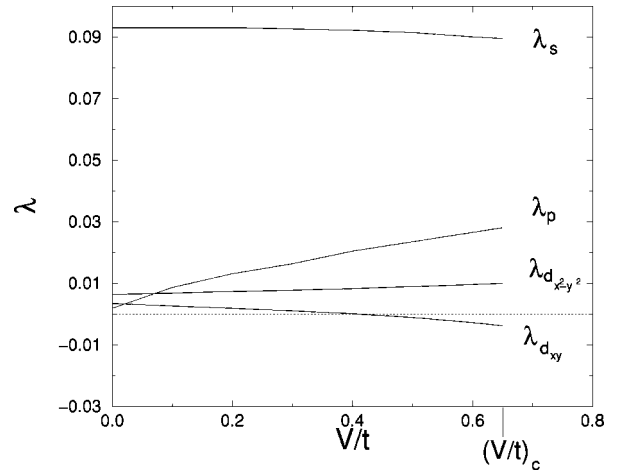
FIG. 15. Schematic plot showing the Fourier transform of the effective potential, $V_{eff}(q_x, q_y)$, for $V/t \approx (V/t)_c$ to real space. $V_{eff}(x,y)$ is understood as follows. A quasiparticle is placed at the origin. For instance, if another quasiparticle is placed also at the origin there is a large repulsion between them due to the large on-site Coulomb repulsion. This is shown by the large positive vertical bar at the origin. At neighboring sites (along the x and y directions) the effective potential between quasiparticles is also positive, i.e., repulsive. However, at the next-nearest-neighbor sites (along the diagonals of the lattice), the potential becomes attractive. This leads to d_{xy} pairing of the quasiparticles.

lead to similar conclusions.[31] Although the eigenvalues are small, our results are nontrivial and show a tendency of the model to Cooper pairing in the d_{xy} channel. Intuitively one would think that superconductivity is less and less favorable when increasing V, due to the repulsion between electrons in neighboring sites. Contrary to this intuition we find that short-range charge fluctuations can mediate pairing close to V_c.

In Fig. 13 we observe that as we increase V, the effective interaction becomes more repulsive at small momentum transfer. On the other hand, they become more attractive for momenta transfer close to (π,π). That d_{xy} symmetry is favored can be more clearly understood from Fig. 15 which shows a schematic plot of the Fourier transform of $V_{eff}(\mathbf{q})$ (see Fig. 13). One sees that the potential is negative for an electron placed at the nearest-neighbor diagonal sites of the lattice while it is positive along the x and y directions. This is in contrast to the effective potential resulting from spin fluctuations which show the opposite behavior. This can be understood from previous calculations on a three-dimensional extended Hubbard model close to half filling within RPA performed by Scalapino, Loh, and Hirsch,[41] which found that the effective potential for charge fluctuations has a *negative* divergence at (π,π) as the transition is approached whereas for spin fluctuations it is positively diverging.[41] Due to the fact that the Fermi surface at one-quarter filling is small [no two points in the Fermi surface are connected by the (π,π) wave vector], the interaction is less effective in inducing pairing as compared to spin fluctuations in nearly antiferromagnetic metals close to half filling.

The T_c values shown in the phase diagram in Ref. 6 are larger than the values that would be obtained for $T_{cd_{xy}}$ from the BCS equation. In Ref. 6 T_c (for each V) was taken to be the temperature below which the coupling $\lambda_{d_{xy}}$ becomes negative. Such a calculation is indicative of superconductivity. However, the appropriate way to obtain T_c is by solving the associated Eliashberg gap equation.

In conclusion, in the present study we find tendencies to superconductivity in the d_{xy} channel mediated by short-range charge fluctuations which appear in the metallic phase close to the charge-ordering instability.

B. Lanczos diagonalization: Binding energies

We have computed the binding energy of two holes for different values of V/t and $U=20t$ on different clusters. The binding energy of two holes for $L=16$ is defined as[43–45]

$$E_B(2 \text{ holes}) = [E(6) - E(8)] - 2[E(7) - E(8)], \quad (37)$$

where $E(N_e)$ is the energy of the system with N_e electrons.

In Fig. 16 we plot the binding energy for different values of V. Initially, as we increase V, the binding energy becomes more positive. This corresponds to the weak-coupling regime where one naively expects that V keeps the quasiparticles farther apart. Further increasing of V closer to the metal-insulator transition but still in the metallic phase leads to a negative binding energy of two holes. From finite-size scaling of the binding energy of clusters up to $L=20$ sites, we
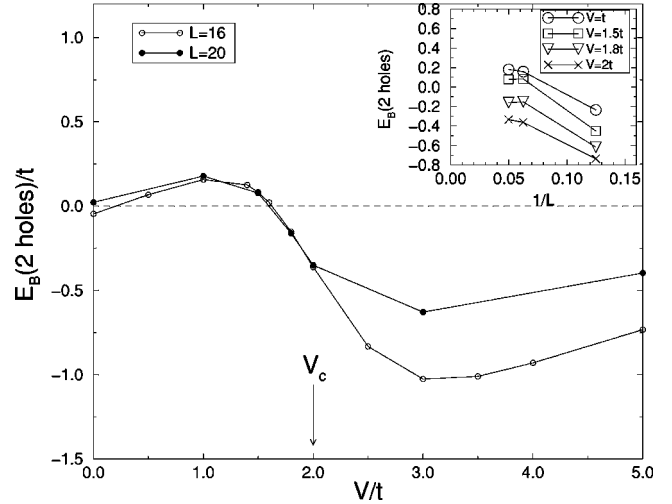

FIG. 16. Binding energy of two holes for different values of V and $U=20t$ from exact diagonalisation calculations on $L=16$ and $L=20$ clusters. Close to the charge-ordering transition, in the range, $V>1.6t$, binding of two holes becomes favorable. V_c denotes the value of V at which the metal-insulator transition is estimated to take place from Lanczos calculations of the Drude weight. Note that the value of V at which E_B (2 holes) becomes negative is robust against increasing the cluster size from $L=16$ to $L=20$. These results are consistent with large-N calculations supporting the possibility of pair formation close to the charge-ordering transition.

find that this happens at about $V\approx1.6t$. This finite-size scaling is shown in the inset of Fig. 16 for values of V close to the metal-insulator transition. Remarkably, the binding energy of two holes changes only slightly in the range of values $t<V<2t$ when going from $L=16$ to $L=20$. However, in the region $V>V_c=2t$, the results change significantly as we increase the size of the cluster from $L=16$ to 20, and the binding energy would eventually extrapolate to a positive value in the thermodynamic limit. It is interesting that this region corresponds to the insulating phase found earlier[11] from Lanczos calculations of the Drude weight. An interpretation of our results can be made based on previous works[44,43] which studied the binding energy of an extended Hubbard model of the high-T_c superconductors close to half filling as a function of V. As V is increased charge fluctuations associated with checkerboard charge ordering increase and the quasiparticles existing at small V gradually dress up with a cloud of checkerboard charge excitations. This leaves signatures in the one-electron dynamical properties as explained in previous sections. Further increasing of V leads to pairing between the quasiparticles mediated by the strong charge fluctuations.[44] Increasing V even further drives the system into the insulating phase.

Summarizing, a definitive conclusion about superconductivity cannot be made from our results. However, it is remarkable that both large-N and Lanczos diagonalization calculations show a similar tendency to pairing of quasiparticles in the metallic phase close to the charge-ordering transition. Large-N theory singles out the d_{xy} symmetry as the preferred pairing channel of the quasiparticles. This symmetry is con-

sistent with the checkerboard charge order present in the region where the Lanczos pairing energy becomes negative.

VI. CONCLUSIONS

In summary, using a combination of large-N and Lanczos techniques we have explored the dynamical properties of the extended Hubbard model at quarter filling. This is motivated by its relevance to a large class of superconducting layered organic molecular crystals. The correlation functions computed from large-N theory and Lanczos techniques are found to be in good agreement. Indeed, close to the charge-ordering transition driven by the intersite Coulomb repulsion, V, several features are found.

(i) The quasiparticle weight $Z_{\mathbf{k}}$ is rapidly suppressed near the charge-ordering transition.

(ii) Spectral density is enhanced at frequencies ranging from t to $3t$, which is also reflected in the optical conductivity.

(iii) From the computation of the electron scattering rate we find Fermi-liquid behavior up to $T \approx T^*$, where T^* does not depend strongly on V. For $T > T^*$ the scattering rate behaves linearly with T.

(iv) From large-N calculations we find that superconductivity with d_{xy} symmetry is favored close to the charge-ordering transition. Exact diagonalization calculations of the binding energy of two holes are consistent with this possibility.

Given our prediction of unconventional superconductivity in the θ and β'' molecular crystals it is desirable that more measurements be made to test for this. The only evidence so far comes from a measurement of the temperature dependence of the London penetration depth of β''-$(BEDT\text{-}TTF)_2SF_5CH_2CF_2SO_3$. It was found to go like T^3 at low temperatures.[46] This is inconsistent with an s-wave state, but also deviates significantly from the linear temperature dependence expected for a d-wave state. On the other hand, the temperature dependence of the heat capacity is consistent with s-wave pairing.[47] Electronic Raman scattering could be used to investigate the symmetry of the superconducting order parameter. For d_{xy} symmetry, Raman scattering in the superconducting state should show, at low frequencies, either ω, ω^3, or ω behavior for B_{1g}, B_{2g}, and, A_{1g} symmetries, respectively.[48]

An important issue to be resolved concerns the role of spin fluctuations in the quarter-filled materials. To first order in $1/N$, the large-N approach used here does not take spin fluctuations into account.[49] Measurements of the nuclear-magnetic-resonance relaxation rate and Knight shift should be done in the metallic phase for the relevant superconductors. If the spin fluctuations are not important there should be no enhancement of the Korringa ratio. This is in contrast to the large enhancements seen in $\kappa\text{-}(BEDT\text{-}TTF)_2X$ superconductors which are close to an antiferromagnetic Mott insulator.[50]

One way to theoretically investigate the role of the antiferromagnetic spin fluctuations that may be present near the charge-ordering transition is as follows. Well into the insulating charge-ordered phase (i.e., for $V \gg t$) it is known that there is an antiferromagnetic exchange interaction $J' = 4t^4/9V^3$ that acts along the *diagonals* of the square lattice.[4] Some remnant of this effect will still be present when there is short-range charge order. This could be modeled by considering a $t - J' - V$ model where the J' acts only along the diagonals. This model could be studied by the same large-N method used previously to study a large family of $t - J - V$ models.[51] There it was found that the superexchange, acting along the vertical and horizontal lattice directions, produced $d_{x^2-y^2}$ superconductivity. Based on that work we anticipate that the effect of the superexchange, which now acts in directions rotated by $45°$, will be to produce d_{xy} superconductivity. Hence, it is possible that charge and spin fluctuations work together cooperatively to produce d_{xy} pairing.

[1] T. Yamauchi, Y. Ueda, and N. Mori, Phys. Rev. Lett. **89**, 057002 (2002).

[2] Y. Onose, Y. Taguchi, T. Ishikawa, S. Shinomori, K. Ishizaka, and Y. Tokura, Phys. Rev. Lett. **82**, 5120 (1999).

[3] T. Ishiguro, K. Yamaji, and G. Saito, *Organic Superconductors*, 2nd ed. (Springer-Verlag, Berlin, 1998).

[4] R.H. McKenzie, J. Merino, J.B. Marston, and O.P. Sushkov, Phys. Rev. B **64**, 085109 (2001).

[5] S. Lefebvre, P. Wzietek, S. Brown, C. Bourbonnais, D. Jérome, C. Mézière, M. Fourmigué, and P. Batail, Phys. Rev. Lett. **85**, 5420 (2000).

[6] J. Merino and R.H. McKenzie, Phys. Rev. Lett. **87**, 237002 (2001).

[7] N.L. Wang, T. Feng, Z.J. Chen, and H. Mori, e-print cond-mat/0211226.

[8] H. Tajima, S. Kyoden, H. Mori, and S. Tanaka, Phys. Rev. B **62**, 9378 (2000).

[9] J. Dong, J.L. Musfeldt, J.A. Schlueter, J.M. Williams, P.G. Nixon, R.W. Winter, and G.L. Gard, Phys. Rev. B **60**, 4342 (1999).

[10] M. Dressel, N. Drichko, J. Schlueter, and J. Merino, Phys. Rev. Lett. **90**, 167002 (2003).

[11] M. Calandra, J. Merino, and R.H. McKenzie, Phys. Rev. B **66**,

195102 (2002), and references therein.

[12] A. Chubukov, D. Pines, and J. Schmalian, *The Physics of Conventional and Unconventional Superconductors*, edited by K.H. Bennemann and J.B. Ketterson (Springer-Verlag, Berlin, 2002).

[13] J. Schmalian, Phys. Rev. Lett. **81**, 4232 (1998); M. Vojta and E. Dagotto, Phys. Rev. B **59**, R713 (1999); H. Kino and K. Kontani, J. Phys. Soc. Jpn. **67**, 3691 (1998); H. Kondo and T. Moriya, *ibid.* **67**, 3695 (1998); T. Jujo, S. Koikegami, K. Yamada, *ibid.* **68**, 1331 (1999); S.W. Tsai and J.B. Marston, Can. J. Phys. **79**, 1463 (2001).

[14] N.D. Mathur, F.M. Grosche, S.R. Julian, I.R. Walker, D.M. Freye, R.K.W. Haselwimmer, and G.G. Lonzarich, Nature (London) **394**, 39 (1998).

[15] I.I. Mazin and D.J. Singh, Phys. Rev. Lett. **82**, 4324 (1999).

[16] J. Hubbard, Proc. R. Soc. London, Ser. A **276**, 238 (1963).

[17] G. Kotliar and J. Liu, Phys. Rev. Lett. **61**, 1784 (1988).

[18] R. Zeyher and A. Greco, Eur. Phys. J. B **6**, 473 (1998); A. Greco and R. Zeyher, Phys. Rev. B **63**, 064520 (2001).

[19] A. Foussats and A. Greco, Phys. Rev. B **65**, 195107 (2002).

[20] P. van Nieuwenhuizen, Phys. Rep. **68**, 1 (1981).

[21] E. Fradkin, *Field Theories of Condensed Matter Systems* (Addison-Wesley, Reading, MA, 1991).

[22] Z. Wang, Int. J. Mod. Phys. B **6**, 155 (1992).

[23] See, for example, D.H. Kim, P.A. Lee, and X.-G. Wen, Phys. Rev. Lett. **79**, 2109 (1997), and references therein.

[24] See, for example, E. Zojer, M. Knupfer, Z. Shuai, J. Fink, J.L. Bredas, H.-H. Hörhold, J. Grimme, U. Scherf, T. Benin cori, and G. Leising, Phys. Rev. B **61**, 16 561 (2000).

[25] M.Z. Hasan, P.A. Montano, E.D. Isaacs, Z.-X. Shen, H. Eisaki, S.K. Sinha, Z. Islam, N. Motoyama, and S. Uchida, Phys. Rev. Lett. **88**, 177403 (2002).

[26] C. Castellani, C. Di Castro, and M. Grilli, Phys. Rev. Lett. **75**, 4650 (1995).

[27] R. Hlubina and T.M. Rice, Phys. Rev. B **51**, 9253 (1995).

[28] Y. Yanase and K. Yamada, J. Phys. Soc. Jpn. **68**, 548 (1999).

[29] Z. Wang, Y. Bang, and G. Kotliar, Phys. Rev. Lett. **67**, 2733 (1991).

[30] A.P. Kampf and J.R. Schrieffer, Phys. Rev. B **42**, 7967 (1990).

[31] E. Dagotto and J. Riera, Phys. Rev. B **46**, 12 084 (1992).

[32] P.F. Maldague, Phys. Rev. B **16**, 2437 (1977).

[33] K. Yakushi, K. Yamamoto, M. Simonyan, J. Ouyang, C. Nakano, Y. Misaki, and K. Tanaka, Phys. Rev. B **66**, 235102 (2002).

[34] J. Ouyang, K. Yakushi, Y. Misaki, and K. Tanaka, Phys. Rev. B **63**, 054301 (2001).

[35] H. Seo, J. Phys. Soc. Jpn. **69**, 805 (2000).

[36] R.T. Clay, S. Mazumdar, and D.K. Campbell, J. Phys. Soc. Jpn. **71**, 1816 (2002).

[37] See A. Georges, G. Kotliar, W. Krauth, and M.J. Rozenberg, Rev. Mod. Phys. **68**, 13 (1996).

[38] M. Rozenberg, G. Kotliar, H. Kajueter, G.A. Thomas, D.H. Rapkine, J.M. Honig, and P. Metcalf, Phys. Rev. Lett. **75**, 105 (1995).

[39] K. Yamamoto (unpublished). See K. Yamamoto *et al.*, Phys. Rev. B **65**, 085110 (2002) for a detailed analysis of vibrational features appearing in optical spectra of θ-$(BEDT-TTF)_2RbZn(SCN)_4$.

[40] This is about half the value of 106 meV found in Ref. 52. However, one should be cautious about taking the Hückel and extended Hückel values as definitive. Based on comparison with results from the local-density approximation it is argued in Ref. 53 that the Hückel methods tend to systematically underestimate the hopping integrals.

[41] D.J. Scalapino, E. Loh, and J.E. Hirsch, Phys. Rev. B **35**, 6694 (1987).

[42] A. Greco and R. Zeyher, Europhys. Lett. **35**, 115 (1996).

[43] J.E. Hirsch, S. Tang, E. Loh, and D.J. Scalapino, Phys. Rev. Lett. **60**, 1668 (1988).

[44] W.H. Stephan, W.v.d. Linden, and P. Horsch, Phys. Rev. B **39**, 2924 (1989).

[45] J.A. Riera and A.P. Young, Phys. Rev. B **39**, 9697 (1989).

[46] R. Prozorov, R.W. Giannetta, J. Schlueter, A.M. Kini, J. Mohtasham, R.W. Winter, and G.L. Gard, Phys. Rev. B **63**, 052506 (2001).

[47] S. Wanka, J. Hagel, D. Beckmann, J. Wosnitza, J.A. Schlueter, J.M. Williams, P.G. Nixon, R.W. Winter, and G.L. Gard, Phys. Rev. B **57**, 3084 (1998).

[48] T.P. Devereaux, A. Virosztek, and A. Zawadowski, Phys. Rev. B **54**, 12 523 (1996).

[49] An alternative approach that treats spin and charge fluctuations on equal footing in the Anderson lattice model can be found in A. Sudbo and A. Houghton, Phys. Rev. B **42**, 4105 (1990).

[50] H. Mayaffre *et al.*, Europhys. Lett. **28**, 205 (1994); S.M. De Soto, C.P. Slichter, A.M. Kini, H.H. Wang, U. Geiser, and J.M. Williams, Phys. Rev. B **52**, 10 364 (1995); A. Kawamoto, K. Miyagawa, Y. Nakazawa, and K. Kanoda, *ibid.* **52**, 15 522 (1995).

[51] M. Vojta, Y. Zhang, and S. Sachdev, Phys. Rev. B **62**, 6721 (2000).

[52] H. Mori, S. Tanaka, T. Mori, A. Kobayashi, and H. Kobayashi, Bull. Chem. Soc. Jpn. **71**, 797 (1998).

[53] J. Merino and R.H. McKenzie, Phys. Rev. B **62**, 2416 (2000).